RSC Advances

PAPER

View Article Online
View Journal | View Issue

Cite this: *RSC Adv.*, 2020, **10**, 8941

TiO_2 nanofibres decorated with green-synthesized $P_{Au/Ag}$@CQDs for the efficient photocatalytic degradation of organic dyes and pharmaceutical drugs†

Anupma Thakur,[ab] Praveen Kumar,[*c] Devinder Kaur,[b] Nagaraju Devunuri,[d] R. K. Sinha[b] and Pooja Devi[*b]

Organic pollutants such as dyes and pharmaceutical drugs have become an environmental menace, particularly in water bodies owing to their unregulated discharge. It is thus required to develop an economically viable and environment-friendly approach for their degradation in water bodies. In this study, for the first time, we report green route-synthesized plasmonic nanostructures (P_M-CQDs (where M: Au and Ag)) decorated onto TiO_2 nanofibers for the treatment of toxic dye- and pharmaceutical drug-based wastewater. P_M-CQDs are efficaciously synthesized using carbon quantum dots (CQDs) as the sole reducing and capping agent, wherein CQDs are derived *via* a green synthesis approach from *Citrus limetta* waste. The characteristic electron-donating property of CQDs played a key role in the reduction of Au^{3+} to Au^0 and Ag^+ to Ag^0 under visible light irradiation to obtain P_{Au}-CQDs and P_{Ag}-CQDs, respectively. Thus, the obtained CQDs, P_{Au}-CQDs, and P_{Ag}-CQDs are loaded onto TiO_2 nanofibers to obtain a P_M-CQD/TiO_2 nanocomposite (NC), and are further probed *via* transmission electron microscopy, scanning electron microscopy and UV-visible spectrophotometry. The degradation of organic pollutants and pharmaceutical drugs using methylene blue and erythromycin as model pollutants is mapped with UV-vis and NMR spectroscopy. The results demonstrate the complete MB dye degradation in 20 minutes with 1 mg mL^{-1} of P_{Au}-CQD/TiO_2 NC, which otherwise is 30 minutes for P_{Ag}@CQD/TiO_2 dose under visible light irradiation. Similarly, the pharmaceutical drug was found to degrade in 150 minutes with P_{Au}-CQD/TiO_2 photocatalysts. These findings reveal the enhanced photocatalytic performance of the green-synthesized Au decorated with TiO_2 nanofibers and are attributed to the boosted SPR effect and aqueous-phase stability of Au nanostructures. This study opens a new domain of utilizing waste-derived and green-synthesized plasmonic nanostructures for the degradation of toxic/hazardous dyes and pharmaceutical pollutants in water.

Received 22nd December 2019
Accepted 31st January 2020

DOI: 10.1039/c9ra10804a

rsc.li/rsc-advances

A. Introduction

Owing to the augmented anthropogenic activities that pose a menace to the environment, particularly water pollutants are the subject of major concern.[1] The unregulated release of industrial waste into water resources is one of the major root causes worldwide for detrimental health effects on living beings.[2] Therefore, the unregulated discharge of these colored effluents and wastewater coming from textile or dye industries has become a serious environmental problem as they pollute surface water and groundwater systems and pose a serious threat to the ecological systems and human health even at a concentration of 1.0 mg L^{-1}.[3,4] Thereby, remediation or removal of these industrial colored effluents from wastewater is significantly vital for a "clean and green" environment. Further, these colored effluents can be classified based on their chemical structures such as acid, base, azo, disperse, anthraquinone, or anionic and cationic.[5] Methylene blue (MB), a cationic dye and widespread industrial pollutant accumulates in the ecosystem and is highly toxic. The main health issues due to the existence of MB in water include eye irritation, vomiting, nausea, and diarrhea.[6] In line with the nature of synthetic commercially used dyes (*i.e.*, anionic and cationic), even the usual biological treatment methodologies are ineffective and futile for their decolorization/degradation.[7] In addition, due to the lack of

[a]*Academy of Scientific and Innovative Research (AcSIR), Ghaziabad-201002, India*
[b]*CSIR-Central Scientific Instruments Organisation, Sector-30 C, Chandigarh-160030, India. E-mail: poojaiitr@csio.res.in*
[c]*School of Materials Science, Indian Association for the Cultivation of Science, Kolkata-700030, India. E-mail: praveen.nitrides@gmail.com*
[d]*Vignan's Foundation for Science, Technology & Research, Guntur, Andhra Pradesh – 522213, India*

† Electronic supplementary information (ESI) available. See DOI: 10.1039/c9ra10804a

regulatory guidelines, awareness, and accessible technical solutions, pharmaceuticals have left their footprints in water resources and have been added to the list of alarming water contaminants. Conferring to the US Environmental Protection Agency, a well-recognized antibiotic, *i.e.*, erythromycin is today in the "Drinking Water Contaminant Candidate List".[8] According to a report, ~100 000 tons of pharmaceuticals drugs are currently in use for treating both the human and veterinary population every year.[9] However, the inappropriate release of pharmaceutical drug waste in the environment has led to environmental distress and severe health effects.[10] Furthermore, the unregulated release of pharmaceutical drugs, mainly antibiotics, into the environment promotes the natural development of antibiotic-resistant pathogens that are harder to treat causing "antimicrobial resistance (AMR)".[10] Thus, in order to degrade these chemical pollutants various research strategies based upon chemical treatments such as reduction, neutralization, oxidation, and ion exchange and physical methods such as precipitation, adsorption, filtration, and reverse osmosis have been devised.[11] Alternatively, the solar light-assisted catalytic degradation of organic pollutants in the presence of a photocatalyst offers their complete degradation and is also beneficial for the treatment of industrial effluents containing dyes and pharmaceutical drugs.[12] In this respect, a wide range of semiconductor materials, including TiO_2, a well-known photocatalyst, has been mostly employed for the degradation of their pollutants owing to their main features including non-toxicity, low cost, biochemical inertness, and photo-stability; however, its wide-bandgap (3.2 eV) limits its efficiency.[13,14] Further, to enhance the photocatalytic activity of TiO_2 by modifying its absorbance towards visible light, several photosensitizers, plasmonic materials, small-bandgap semiconductors, and metallic and non-metallic doping agents have been reconnoitred.[15–17] For instance, modified TiO_2-based photocatalysts are largely investigated towards photocatalytic degradation of pharmaceutical drugs under the UV-visible irradiation.[18–20] More recently, due to tunable optical properties, non-toxicity, high catalytic activity, chemical stability, large-scale production, water solubility, easy functionalization, and low cost, the applicability of carbonaceous nanostructures has been explored as a photosensitizer.[21–28] However, the practical realizations of carbon quantum dots (CQDs) as photosensitizers for water pollutant remedial is yet in the progressive stage, as summarised in ESI Table 1† and need more comprehensive and systematic investigations.[23] Owing to the visible light absorption, the up-conversion and electron-donating property of CQDs, and the photocatalytic activity of the CQD-anchored TiO_2 composites has been revealed to enhance in the reported literature.[29–32]

Besides, plasmonic nanostructures are widely utilized as active sensitizers for visible light; however, they are mainly derived from a synthetic route. Similarly, in the recent past, Ag-loaded zinc/aluminium-layered double hydroxide nanocomposites, $Ag/AgIn_5S_8$ nanoparticles and $BiOCl/AgCl/BiVO_4$ photocatalysts have been investigated for the photocatalytic degradation of pharmaceutical drugs, and the results showed that their enhanced photocatalytic activity is attributed to the boosted surface plasmon resonance (SPR) effect of Ag nanostructures.[33–35] Carbon quantum dots can function not only as an efficient visible light photocatalyst but also as a multifunctional component in a photocatalyst design to stimulate wider absorption spectrum and separation of photogenerated charge carriers (electrons and holes) as well as to stabilize semiconductor-based photolysis. However, metal nanoparticles (Au, Ag, *etc.*) are known to possess catalytic reaction sites for selective oxidation reactions and surface plasma resonance absorption that induces good photocatalytic abilities. Herein, we report the design of an efficient tunable photocatalyst based on the composite of $P_{M(Au,Ag)}$@CQD/TNF nanocomposites, which enhance light absorption and the production of active oxygen species, which collectively lead to their high-performance photocatalytic activity as compared to pristine metal nanoparticles.[36–39] In view of literature, as portrayed in ESI Fig. S1,† plasmonic carbon quantum dots as photosensitizers have not yet been investigated for the photocatalytic degradation of pharmaceutical drugs to the best of our knowledge.[40] However, in present study we have synthesized plasmonic nanostructures from green-synthesized CQDs (derived from the waste pulp of *Citrus limetta*), and utilized CQDs, Au-CQDs, and Ag-CQDs as photosensitizers for TiO_2 nanofibers, a UV active catalyst, to obtain the P_M (Au or Ag)-CQD/TiO_2 nanocomposite (NC). Thus, waste CQD-derived plasmonic nanostructures are used as an effectual photosensitizer for the photocatalytic degradation of methylene blue dye and erythromycin drug. We have mainly attributed the significant improvement of photocatalytic performance to the synergistic effects in NCs, which enhance light absorption due to their surface plasmon resonance (SPR) effect.[41–43]

B. Experimental section

A. Materials

All the chemicals used for the synthesis were of analytical grade and used directly without any purification. CQDs were synthesized using the waste pulp of *Citrus limetta*. TiO_2 nanofibres were prepared using polyvinylpyrrolidone (PVP, average MW 1 300 000), ethanol, acetic acid, and titanium tetraisopropoxide ($Ti[OCH(CH_3)_2]_4$) procured from Loba Chemie. For the plasmonic nanostructure and CQD synthesis: silver nitrate and chloroauric acid were procured from Sigma Aldrich. Methylene blue (MB) that was studied for dye degradation experiments was also procured from Sigma Aldrich. Pharmaceutical drug, erythromycin, for pharmaceutical degradation experiments was procured from the nearby medical store. Millipore corporation grade water system (Milli-Q, 18.2 MΩ) was used to perform all studies and preparation of standard solutions.

B. Instrumentation

The optical characterization of the as-synthesized P_M-CQD/TiO_2 is performed on a UV-vis (Hitachi U-3900-H) spectrophotometer. The morphologies were probed *via* high-resolution transmission electron microscopy (HR-TEM, H-7500, Hitachi Ltd., Japan) and scanning electron microscopy (SEM, Hitachi S-4300).

C. Synthesis $P_{Au/Ag}$-CQD/TiO_2 nanofibers

CQDs were synthesized using the waste pulp of *Citrus limetta* as a green carbon precursor.[44] The present finding reveals a more accessible one-step synthesis methodology for the synthesis of water-soluble waste-derived plasmonic nanostructures. Au-CQDs were synthesized by the continuous stirring of the $HAuCl_4$ (used as a precursor) (1 mM) and CQD (0.5 M) solution in the ratio of 1 : 9 at room temperature under visible light irradiation for a duration of 20 minutes. The reaction color changes from pale yellow to pinkish red, which indicated the formation of P_{Au}-CQDs. As CQDs are known as worthy electron-donating materials, accordingly they are devised to reduce Au^{3+} to Au^0 under visible light irradiation. Moreover, the presence of hydrophilic functionalities such as –OH, –COOH on the surface of CQDs promote the reduction and stabilization of Au-CQDs.[45] Similarly, P_{Ag}-CQDs were synthesized by the addition of a silver nitrate precursor (1 mL, 0.01 M) to CQDs (3 mL, 0.5 M) along with an ammonia (0.5 mL, 0.06 M) solution at room temperature. The P_M-CQD (M: Au or Ag)/TiO_2 nanofiber-based nanocomposites were synthesized by loading 150 μL of each P_M-CQDs (M: Au or Ag) atop electro-spunned TiO_2 nanofibers (TNFs), resulting in the formation of P_{Au}-CQD/TiO_2 and P_{Ag}-CQD/TiO_2 nanofibers. Thereafter, the photocatalytic activities of the as-synthesized P_{Au}-CQD/TiO_2 and P_{Ag}-CQD/TiO_2 nanofibers were examined towards methylene blue (MB) and pharmaceutical drug degradation.

D. Photocatalytic treatment application

These composites were assessed for their photocatalytic activities for methylene blue (MB) degradation under UV-visible light irradiation (250 W lamp). The reaction was performed in a photocatalytic reaction cell, containing a suspension of the as-synthesized catalyst $P_{Au/Ag}$-CQD/TiO_2 in the MB dye solution, and at first, kept in dark for a time interval of 30 minutes in order to acquire the equilibrium in adsorption–desorption characteristics. The equilibrated solution then exposed to UV-visible light irradiation with constant stirring. Samples were collected after every five minutes until the complete degradation of MB, examined from the absorption spectra recorded for the MB dye (at 664 nm) *via* a conventional UV-vis spectrophotometer. The resultant by-products from the photocatalytic degradation of MB were analysed *via* NMR spectroscopy. *In lieu* of promising results obtained with MB, we also studied $P_{Au/Ag}$-CQD/TiO_2 for the pharmaceutical drug, erythromycin, and degradation under solar irradiation. The reaction was performed in a glass vial, containing a suspension of the as-synthesized catalyst $P_{Au/Ag}$-CQD/TiO_2 and the pharmaceutical drug, erythromycin, dissolved in water solution. At first, the solution was kept in dark to acquire the equilibrium in adsorption–desorption characteristics. The equilibrated solution was then exposed to solar irradiation. Samples were collected after every thirty minutes until the complete (~100%) degradation of a pharmaceutical drug, which was mapped from the absorption spectra recorded for pharmaceutical drugs using a UV-vis spectrophotometer.

C. Results & discussion

A. Characterization of P_M-CQD/TiO_2-based nanocomposites

A systematic approach for the synthesis of plasmonic nanostructures, *i.e.*, $P_{Au/Ag}$-CQDs, using the waste pulp of *Citrus limetta* derived CQDs as the sole reducing/capping agent, with the vital perspective to use these waste-derived plasmonic nanostructures as an effectual photosensitizer is presented in Scheme 1.

These green-synthesized plasmonic nanostructures are further loaded onto TiO_2 nanofibers to obtain $P_{Au/Ag}$-CQD/TiO_2 nanocomposites (NC) for the photocatalytic degradation of MB dye and erythromycin drug. The morphological and structural characteristics of P_M-CQDs were analysed *via* high-resolution transmission electron microscopy (HR-TEM). Fig. 1(a and b) depict the morphological characteristics of the as-synthesized P_{Ag}-CQDs and P_{Au}-CQDs, wherein the HR-TEM micrographs reveal the spherical morphology of nanostructures with a typical diameter of ~10 nm. The HR-TEM images also show that the obtained particles are well-dispersed. The diffraction rings from the SAED patterns portray the existence of Ag and Au associated Bragg reflections, which are indexed according to the (111), (200), (220), (311) and (222) reflections of face-centered cubic (FCC) Ag and Au.[46] Fig. 1(c) represents the optical absorption characteristics recorded for P_{Au}-CQD/TiO_2 and P_{Ag}-CQD/TiO_2 NCs. The signature of UV-vis absorption characteristics is observed and the bandgap is calculated to be 2.6 eV and 2.4 eV for P_{Au}-CQD/TiO_2 and P_{Ag}-CQD/TiO_2 NCs, respectively, which is in line with the surface plasmon resonance peaks associated with Au and Ag nanoparticles.[47,48] In addition, the SEM micrographs represent the fibrous nature of TiO_2 nanofibers, which were used to load P_{Ag}-CQDs and P_{Au}-CQDs for the photocatalytic degradation study of organic pollutants (ESI Fig. S2†). The TEM images of P_M-CQDs (where M: Au and Ag) decorated onto TiO_2 nanofibers are presented in ESI Fig. S3.†

B. Photocatalytic degradation of the MB dye and erythromycin drug with P_M-CQD/TiO_2 NCs

The present work, for the first time, reports green-synthesized plasmonic nanostructures as an active photosensitizer for the

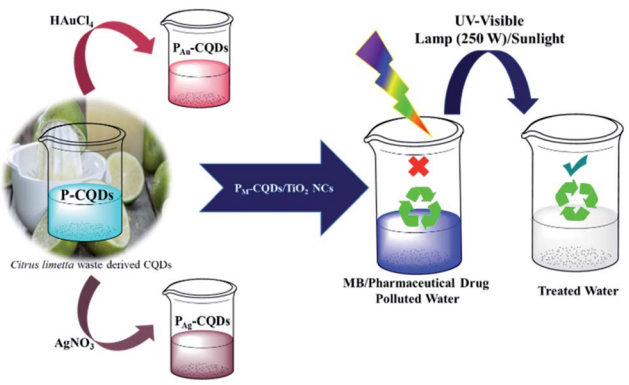

Scheme 1 Schematic showing the facile synthesis of P_M-CQD-based NCs and their application as an effectual photocatalyst for the degradation of methylene blue (MB) dye and pharmaceutical drug.

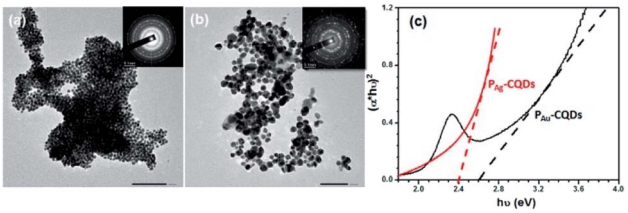

Fig. 1 HR-TEM micrograph of (a) P_{Ag}-CQDs and (b) P_{Au}-CQDs, and (c) optical characterizations of P_M-CQDs.

photocatalytic dye and pharmaceutical drug degradation with TiO_2 nanofibers, over widely-known applications of CQDs as photosentitizers.[49–55] The photocatalytic activity of P_M-CQD/TiO_2 NC was studied for the degradation of MB dye under a UV-visible light source (250 W). MB exhibits characteristic absorption peaks at 609 nm and 663 nm, and the change in its absorption characteristics w.r.t. photocatalyst loading, time, and dye concentration were mapped using a conventional UV-vis spectrophotometer.[56] ESI Fig. S4† presents a sequence of UV-vis absorption spectra of the MB dye (10 ppm) suspension in the presence of the different loading concentrations, *i.e.*, 1 mg mL^{-1} and 0.5 mg mL^{-1}, of the P_{Au}-CQD/TiO_2 and P_{Ag}-CQD/TiO_2 catalysts, respectively.

The MB suspension was collected at different time intervals (*i.e.*, 5, 10, and 20 min) w.r.t. different concentrations of catalysts, and the associated decrease in absorption and visual colorimetric characteristic of MB (10 ppm) was observed with an increase in time. The high loading of catalyst, *i.e.*, 1 mg mL^{-1} showed a better degradation rate compared to 0.5 mg mL^{-1}. This is because as the loading of the P_M-CQD/TiO_2 photocatalysts increased, the tendency of active sites at the surface of photocatalysts also augmented, thus exhibiting the boosted MB dye degradation efficiency. Also, with increase in time, MB degradation was higher in the presence of the P_M-CQD/TiO_2 catalyst through the generation of free radicals under the light. Further, the MB dye (10 ppm) degradation mechanistic (Fig. 2(a)) as well as degradation efficiency (Fig. 2(b)) were also studied based on the changes in the absorption intensity of the dye with respect to the concentrations of catalyst (1 mg mL^{-1} and 0.5 mg mL^{-1}). The degradation efficiency of the P_M-CQD/TiO_2 photocatalysts was calculated using the expression given below in eqn (1):

$$\text{Degradation efficiency}(\%) = \frac{C_0 - C_t}{C_0} \times 100 \qquad (1)$$

Here, C_0 and C_t are attributed to the concentrations of dye before and after degradation at time t. The degradation efficiency of the MB dye with the P_M-CQD/TiO_2 photocatalysts is higher than that of controls that reveals the enhanced photocatalytic performance of NCs. It is further observed that the degradation rate of MB is higher with P_{Au}-CQD/TiO_2 photocatalysts over P_{Ag}-CQD/TiO_2, which could be assigned to the stability of Au nanostructures over Ag nanostructures, and thus the retained SPR effect required for dye degradation. The degradation efficiency of the MB dye with the P_{Au}-CQD/TiO_2

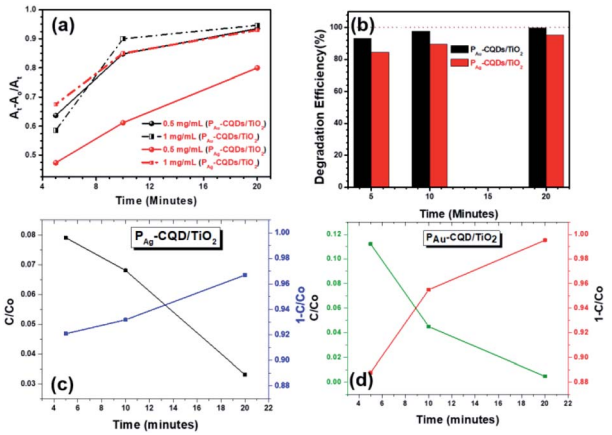

Fig. 2 (a) Absorption characteristics of MB (10 ppm) with respect to the PM-CQD/TiO_2 catalyst concentrations (1 mg mL^{-1} and 0.5 mg mL^{-1}) w.r.t. degradation reaction, (b) degradation efficiency and (c and d) half-life measurements of MB dye for P_{Ag}-CQD/TiO_2 and P_{Au}-CQD/TiO_2, respectively.

photocatalysts is found to be ~96% in comparison to P_{Ag}-CQD/TiO_2 for an irradiation time of 20 minutes. The half-life measurements of the MB dye, *i.e.*, the time interval for which half of the MB dye gets degraded in the presence of the photocatalyst was calculated by the observed degradation efficiency characteristics in terms of 1 C/C_0 and C/C_0 and was found to be 8 and 13 minutes for P_{Au}-CQD/TiO_2 and P_{Ag}-CQD/TiO_2, respectively, (Fig. 2(c) and (d)). The degradation rate of the MB dye in accordance with half-life measurements of the MB dye, *i.e.*, 8 min in the presence of P_{Au}-CQD/TiO_2 denotes the better degradation kinetics with P_{Au}-CQD/TiO_2. These preliminary studies showed that P_{Au}-CQD/TiO_2 exhibited a boosted photocatalytic activity as compared to P_{Ag}-CQD/TiO_2 towards the MB dye degradation. Thereafter, detailed studies were performed with P_{Au}-CQD/TiO_2 to evaluate their practical usage. ESI Fig. S5† presents the effects of the MB dye concentration, *i.e.*, (a) 1 ppm, and (b) 20 ppm, on the optimized P_{Au}-CQD/TiO_2 photocatalyst concentration as a function of irradiation time. The results manifest that the photocatalyst could effectively degrade the MB dye up to 20 ppm within the 20 min of irradiation.

The reusability of the P_{Au}-CQD/TiO_2 photocatalyst was also assessed (ESI Fig. S6†) which revealed that the photocatalytic activities of the recycled P_{Au}-CQD/TiO_2 catalysts slightly decreased after several cycles. The pseudo-first-order degradation kinetics for the MB dye degradation using the P_{Au}-CQD/TiO_2 catalyst was determined using eqn (2):

$$\ln \frac{C}{C_0} = -k_{obs}t \qquad (2)$$

Here, k is the observed rate constant (min^{-1}) corresponding to the first-order kinetics reaction; C and C_0 are the concentrations of the MB dye before and after light irradiation for t, time interval, respectively. The rate constants were deliberated using linear fitted plots of $\ln \frac{C}{C_0}$ *versus* t, the time interval of reaction grounded on the MB dye degradation curves by the

approximation of the slope of a line. Further, with the implementation of the Arrhenius equation, the observed rate constants were graphed logarithmically to the reciprocal of temperature, from which a linear relationship was obtained. Thus, activation energy was calculated using the Arrhenius plot:

$$\ln\ k_{obs} = -\frac{E_a}{RT} + \ln A_o \quad (3)$$

where E_a is the Arrhenius activation energy (kJ mol^{-1}), R is the gas constant (8.314 J mol^{-1} K^{-1}), T is the temperature in Kelvin (K), ln A_o is the y-intercept, k_{obs} is the degradation rate constant. The degradation kinetics for the MB dye using the P_{Au}-CQD/TiO_2 photocatalyst was witnessed to follow the pseudo-first-order kinetics model, as shown in ESI Fig. S7(a and b).† On the other hand, E_a, the activation energy for MB dye degradation using the P_{Au}-CQD/TiO_2 photocatalyst was calculated to be 8.26 kJ mol^{-1} using the Arrhenius equation, as shown in ESI Fig. S8.† The presented photocatalyst P_M-CQD/TiO_2 subsidizes in the concentrated absorption of the visible light region to reap an electron–hole pair that consequently enriches the photocatalytic activity. The light-harvested electron–hole pairs are ensnared by the surface at the P_M-CQD/TiO_2 catalyst to generate $^{\bullet}$OH radicals. These $^{\bullet}$OH radicals importantly participate in the oxidization of the MB dye compounds into other eco-friendly by-products. In addition, the dissolved O_2 molecules produce superoxide radical anions, O^{2-},[57] which further speed up the dye degradation process. The following listed equations summarize the mechanism of photocatalytic degradation of MB using P_M-CQD/TiO_2 as photocatalyst:

$$P{-}CQD/TiO_2 + h\nu \rightarrow e^- + h^+ \quad (4)$$

$$h^+ + MB_{dye} \rightarrow MB^{\bullet}_{dye} \rightarrow \text{oxidation of dye} \quad (5)$$

$$h^+ + H_2O \rightarrow H^+ + {}^{\bullet}OH \quad (6)$$

$$h^+ + OH^- \rightarrow H^+ + {}^{\bullet}OH \quad (7)$$

$${}^{\bullet}OH + MB_{dye} \rightarrow \text{degradation of } MB_{dye} \quad (8)$$

The photodegraded by-products of MB-P_{Au}-CQD/TiO_2 within 20 min under a UV-visible light source (250 W) are further assessed *via* proton nuclear magnetic resonance (^{1}H-NMR). The ^{1}H-NMR analysis presents the six aliphatic protons of MB (chemical structure displayed in Fig. 3(a)) at the chemical shift from 2.84 to 3.43 ppm and six aromatic protons exhibited signals at 4.94, 7.96 and 8.01 ppm, as portrayed in Fig. 3(b). The ^{1}HNMR analysis thus showed the complete degradation of the aromatic framework of the MB dye, as shown in Fig. 3(a–c). As there is no significant character of degraded molecules left in the supernatant water sample as analysed by protons signal in ^{1}H-NMR reveals the complete degradation of the aromatic structure of the MB dye.

Fascinated by the excellent photocatalytic activity of green-synthesized plasmonic nanostructures decorated TiO_2 NC, we also studied this material for a preliminary investigation for erythromycin drug degradation under the same condition as the above studies for the developed material composite.[18,58]

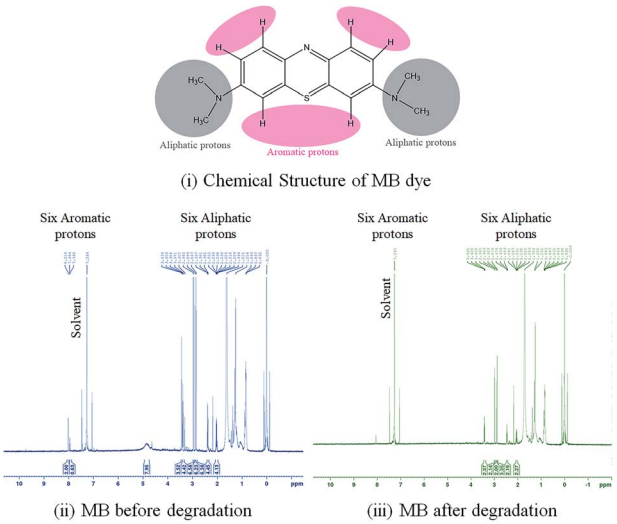

Fig. 3 (a) Chemical structure of the MB dye and ^{1}H-NMR spectra for the (b) MB dye (b) before and (c) after degradation.

Fig. 4 presents a sequence of the UV-vis absorption spectra of pharmaceutical drug (10 ppm) suspension in the presence of the P_{Au}-CQD/TiO_2 and P_{Ag}-CQD/TiO_2 catalysts, respectively.

The pharmaceutical drug suspension was collected at different time intervals (*i.e.*, 30, 60, 90, 120 and 150 min). The subsequent decrease in the absorption peak intensity and color (inset) of the drug correlates to degradation by P_M-CQD/TiO_2 *via* the mechanism proposed for MB degradation. The change in the absorption intensity w.r.t. control, *i.e.*, TiO_2 nanofibers alone reveal that the photocatalytic performance of the composite is higher than that of controls (ESI Fig. S9†). The generated electron–hole pairs under solar irradiation are trapped by the surface of the P_M-CQD/TiO_2 catalyst to produce OH^- radicals. The hydroxyl radical oxidizes the pharmaceutical drug into other non-harmful by-products. Moreover, the dissolved O_2 molecules encountered with the excited electrons also produces superoxide radical anions, O^{2-},[57] to further speed up pharmaceutical drug degradation. Following the relation presented in eqn (1), the degradation efficiency of the P_M-CQD/TiO_2 photocatalysts for erythromycin is shown in Fig. 5(a), which clearly shows the higher rate for P_{Au}-CQD/TiO_2 over P_{Ag}-CQD/TiO_2. The half-life measurements of the pharmaceutical drug were found

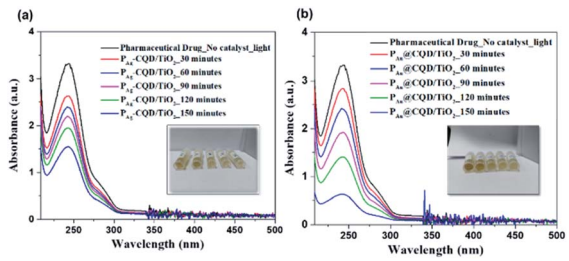

Fig. 4 Absorption spectra of the pharmaceutical drug (10 ppm) at varied time intervals on incubation with 1 mg mL^{-1} of (a) P_{Ag}-CQD/TiO_2 and (b) P_{Au}-CQD/TiO_2 catalyst.

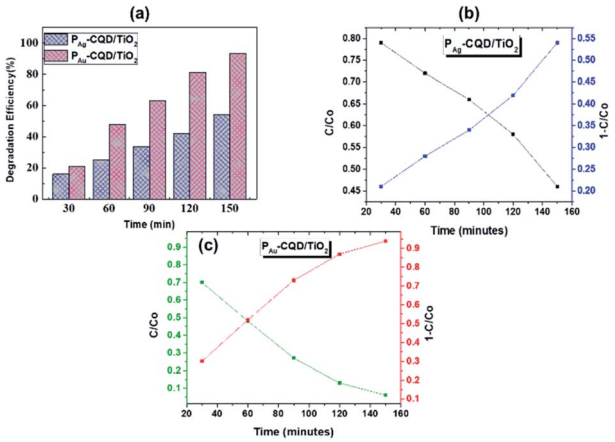

Fig. 5 (a) Degradation efficiency and (b and c) half-life measurements for erythromycin (10 ppm) for P_{Ag}-CQD/TiO_2 and P_{Au}-CQD/TiO_2, respectively.

to be 60 and 108 min for P_{Au}-CQD/TiO_2 and P_{Ag}-CQD/TiO_2, respectively, as shown in Fig. 5(b and c).

As observed from the pharmaceutical drug degradation results, P_{Au}-CQD/TiO_2 again retained the enhanced photocatalytic activity as compared to P_{Ag}-CQD/TiO_2 for the reasons discussed earlier. The time-dependent photoluminescence studies relate to the charge carrier lifetime that shows a direct relationship with the relative photonic efficiency of the photocatalytic activity. Decorating CQDs with metal (Au and Ag) nanoparticles aids electron transfer and creates electron traps in the form of oxygen vacancies on the surface of TiO_2 nanofibers. Owing to the efficient photocatalytic activity of P_{Au}@-CQDs, it is also observed from their time-dependent photoluminescence spectra that these composites show a longer lifetime (~1.0216 ns) of the photogenerated charge carrier, revealing greater charge separation ability (ESI Fig. S10†). A similar effect is observed in literature.[59,60]

To further elucidate the photodegradation process, the total organic carbon (TOC) content of methylene blue (MB) and photodegraded methylene blue dye were found to be 44.99 mg L^{-1} and 18.44 mg L^{-1}, respectively. Similarly, the TOC of pharmaceutical drug and photodegraded pharmaceutical drug was found to be 2440 mg L^{-1} and 319.1 mg L^{-1}, respectively. The plausible photoreaction mechanism and reaction pathways for the photo-induced degradation of the MB dye and pharmaceutical drug are schematically illustrated in Scheme 2. Based on the above experimental results, the photocatalytic mechanism of the P_M-CQD/TiO_2 hybrid composites is proposed and can be understood as follows. The optical band gap was calculated from the Tauc plot $[(\alpha h\nu)^{1/2}$ *vs.* $h\nu]$, where α, h, and ν are absorption coefficient (known from absorption spectra), plank constant and light frequency, respectively. TiO_2 having a large bandgap (3.2 eV) can only absorb the UV light spectrum and does not absorb visible light. On the contrary, the bandgap for CQDs was found to be in the range of ~2.4–2.6 eV, which makes them absorb the visible light.[32] P_M-CQDs further enhance the visible light absorption due to the well-defined

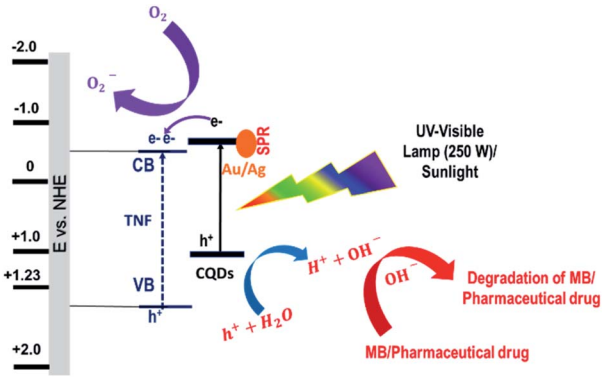

Scheme 2 Schematic showing proposed mechanism for the MB dye and pharmaceutical drug degradation using P_M-CQD/TiO_2.

surface plasmon resonance (SPR) effect. When TiO_2 is decorated with these P_M-CQDs, the conduction band of CQDs well aligns with TiO_2, which is responsible for harvesting visible light and inject excited electrons efficiently into the conduction band (CB) of TiO_2. Further, these electrons travel to the active surface of TiO_2 and react with the adsorbed oxygen to generate reactive superoxide radical anion O_2^-, while the photogenerated holes are responsible for oxidizing the organic molecules in the MB dye/pharmaceutical drug by reacting with OH^- radicals. These succeeding continuous reduction and oxidation reactions on the P_M-CQD/TiO_2 electrodes are mainly responsible for the efficient degradation of the MB dye and pharmaceutical drug.

As observed from the degradation results of organic pollutants, P_{Au}-CQD/TiO_2 showed the boosted photocatalytic activity as compared to P_{Ag}-CQD/TiO_2 towards the MB dye degradation. The vital perspective of the present finding to use this waste-derived plasmonic nanostructure as an effectual photocatalyst for the degradation of organic pollutants (methylene blue (MB) dye and pharmaceutical drug, *i.e.*, erythromycin), can be further explored for the practical utility of this catalyst.

D. Conclusions

In summary, green-synthesized carbon dots were utilized to derive plasmonic nanostructures ($P_{Au/Ag}$-CQDs) in one-step reduction under visible light and are used as an efficient photosensitizer for TiO_2 nanofiber to obtain $P_{Ag/Au}$-CQD/TiO_2 nanocomposites. After structural and optical characterizations, the as-synthesized NCs were investigated as efficient photocatalysts for organic pollutant degradation using methylene blue and erythromycin as the mode dye and drug, respectively. The P_{Au}-CQD/TiO_2 photocatalyst is found to efficiently degrade dye and drug in 20 and 150 min, respectively, under an optimized catalyst loading (1 mg mL^{-1}). The retained SPR effect of Au nanostructures owing to their stability over Ag nanostructures is ascribed to their observed excellent photocatalytic performance. This study paves the usage of waste-derived plasmonic nanostructures as an effectual photosensitizer for organic pollutant degradation in water.

Conflicts of interest

The authors declare no financial and ethical conflict of interest on work reported.

Acknowledgements

The authors acknowledge the constant support received from the Director, CSIR-CSIO, Chandigarh, and IACS-Kolkata. A. T. acknowledges DST-INSPIRE Fellowship from DST for her doctoral study. P. K. acknowledges SERB Project "ECR/2018/001491" and INSPIRE Faculty "IFA13-PH-51" for financial support. The preliminary studies performed by Jasneet Kaur and Abhishek Anand are also acknowledged. Authors further acknowledge, S. Bagchi, for providing electro-spunned TNF.

References

1 M. M. Mekonnen and A. Y. Hoekstra, *Water Resour. Res.*, 2018, **54**, 345–358.
2 S. Thakur and M. Chauhan, in *Water Quality Management*, Springer, 2018, pp. 117–129.
3 S. Sangon, A. J. Hunt, T. M. Attard, P. Mengchang, Y. Ngernyen and N. Supanchaiyamat, *J. Clean. Prod.*, 2018, **172**, 1128–1139.
4 M. Gavrilescu, K. Demnerová, J. Aamand, S. Agathos and F. Fava, *New Biotechnol.*, 2015, **32**, 147–156.
5 S. Markandeya and D. Mohan, *Environ. Toxicol.*, 2017, **11**, 72–89.
6 G. Elango and S. M. Roopan, *J. Photochem. Photobiol., B*, 2016, **155**, 34–38.
7 V. Gupta, S. Khamparia, I. Tyagi, D. Jaspal and A. Malviya, *Global J. Environ. Sci. Manage.*, 2015, **1**, 71–94.
8 D. A. Seehusen and J. Edwards, *J. Am. Board Fam. Med.*, 2006, **19**, 542–547.
9 P. Pierrat, R. Wang, D. Kereselidze, M. Lux, P. Didier, A. Kichler, F. Pons and L. Lebeau, *Biomaterials*, 2015, **51**, 290–302.
10 X. Shi, K. Y. Leong and H. Y. Ng, *Bioresour. Technol.*, 2017, **245**, 1238–1244.
11 S. Mondal, M. K. Purkait and S. De, *Advances in Dye Removal Technologies*, Springer, 2018.
12 P. A. K. Reddy, P. V. L. Reddy, E. Kwon, K.-H. Kim, T. Akter and S. Kalagara, *Environ. Int.*, 2016, **91**, 94–103.
13 S. S. Priya, A. Deshpande and R. Dwarakanath, *International Journal of Research in Engineering and Technology*, 2015, **4**, 200–204.
14 S. A. Anjugam Vandarkuzhali, N. Pugazhenthiran, R. Mangalaraja, P. Sathishkumar, B. Viswanathan and S. Anandan, *ACS Omega*, 2018, **3**, 9834–9845.
15 W. Fang, M. Xing and J. Zhang, *J. Photochem. Photobiol., C*, 2017, **32**, 21–39.
16 J. Shu, Z. Qiu, S. Lv, K. Zhang and D. Tang, *Anal. Chem.*, 2018, **90**, 2425–2429.
17 Y. Shiraishi, J. Imai, N. Yasumoto, H. Sakamoto, S. Tanaka, S. Ichikawa and T. Hirai, *Langmuir*, 2019, **35**(16), 5455–5455.
18 M. Ahmadi, H. R. Motlagh, N. Jaafarzadeh, A. Mostoufi, R. Saeedi, G. Barzegar and S. Jorfi, *J. Environ. Manag.*, 2017, **186**, 55–63.
19 H. Yang, T. An, G. Li, W. Song, W. J. Cooper, H. Luo and X. Guo, *J. Hazard. Mater.*, 2010, **179**, 834–839.
20 H. Yang, G. Li, T. An, Y. Gao and J. Fu, *Catal. Today*, 2010, **153**, 200–207.
21 K. S. Fernando, S. Sahu, Y. Liu, W. K. Lewis, E. A. Guliants, A. Jafariyan, P. Wang, C. E. Bunker and Y.-P. Sun, *ACS Appl. Mater. Interfaces*, 2015, **7**, 8363–8376.
22 M. Radzig, O. Koksharova, I. Khmel, V. Ivanov, K. Yorov, J. Kiwi, S. Rtimi, E. Tastekova, A. Aybush and V. Nadtochenko, *Nanomaterials*, 2019, **9**, 217.
23 S.-S. Yi, J.-M. Yan, B.-R. Wulan, S.-J. Li, K.-H. Liu and Q. Jiang, *Appl. Catal., B*, 2017, **200**, 477–483.
24 P. Serp, M. Corrias and P. Kalck, *Appl. Catal., A*, 2003, **253**, 337–358.
25 S. Ghosh, N. A. Kouamé, L. Ramos, S. Remita, A. Dazzi, A. Deniset-Besseau, P. Beaunier, F. Goubard, P.-H. Aubert and H. Remita, *Nat. Mater.*, 2015, **14**, 505.
26 S. Ghosh, T. Maiyalagan and R. N. Basu, *Nanoscale*, 2016, **8**, 6921–6947.
27 S. Ghosh, H. Remita and R. N. Basu, *Appl. Catal., B*, 2018, **239**, 362–372.
28 H. Remita, M. G. M. Medrano and C. Colbeau-Justin, Effect of Modification of TiO_2 with Metal Nanoparticles on its Photocatalytic Properties Studied by Time-Resolved Microwave Conductivity, in *Visible Light-Active Photocatalysis: Nanostructured Catalyst Design, Mechanisms, and Applications*, Wiley, 2018, pp. 129–164, ISBN: 3527342931.
29 R. Miao, Z. Luo, W. Zhong, S.-Y. Chen, T. Jiang, B. Dutta, Y. Nasr, Y. Zhang and S. L. Suib, *Appl. Catal., B*, 2016, **189**, 26–38.
30 P. S. Saud, B. Pant, A.-M. Alam, Z. K. Ghouri, M. Park and H.-Y. Kim, *Ceram. Int.*, 2015, **41**, 11953–11959.
31 N. A. Travlou, M. Algarra, C. Alcoholado, M. Cifuentes-Rueda, A. M. Labella, J. M. Lázaro-Martínez, E. Rodríguez-Castellón and T. J. Bandosz, *ACS Appl. Bio Mater.*, 2018, **1**, 693–707.
32 A. Thakur, P. Devi, S. Saini, R. Jain, R. K. Sinha and P. Kumar, *ACS Sustainable Chem. Eng.*, 2018, **7**, 502–512.
33 A. Elhalil, R. Elmoubarki, M. H. Sadiq, M. Abdennouri, Y. Kadmi, L. Favier, S. Qourzal and N. Barka, *Desalin. Water Treat.*, 2017, **94**, 254–262.
34 R. Akbarzadeh, A. Asadi, P. O. Oviroh and T.-C. Jen, *Materials*, 2019, **12**, 2297.
35 F. Deng, L. Zhao, X. Luo, S. Luo and D. D. Dionysiou, *Chem. Eng. J.*, 2018, **333**, 423–433.
36 S. Bera, S. Ghosh, S. Shyamal, C. Bhattacharya and R. N. Basu, *Sol. Energy Mater. Sol. Cells*, 2019, **194**, 195–206.
37 S. Ghosh, D. Rashmi, S. Bera and R. N. Basu, *Int. J. Hydrogen Energy*, 2019, **44**, 13262–13272.
38 S. Ghosh, A. K. Mallik and R. N. Basu, *Sol. Energy*, 2018, **159**, 548–560.
39 P. Kar, S. Sardar, B. Liu, M. Sreemany, P. Lemmens, S. Ghosh and S. K. Pal, *Sci. Technol. Adv. Mater.*, 2016, **17**, 375–386.

40 W. o. Science, *Photocatalytic Pharmaceutical Degradation*, http\\www.webofknowledge.com.
41 L. Zhou, D. F. Swearer, C. Zhang, H. Robatjazi, H. Zhao, L. Henderson, L. Dong, P. Christopher, E. A. Carter and P. Nordlander, *Science*, 2018, **362**, 69–72.
42 X. Liang, P. Wang, M. Li, Q. Zhang, Z. Wang, Y. Dai, X. Zhang, Y. Liu, M.-H. Whangbo and B. Huang, *Appl. Catal., B*, 2018, **220**, 356–361.
43 M. Zhao, H. Xu, S. Ouyang, H. Tong, H. Chen, Y. Li, L. Song and J. Ye, *ACS Catal.*, 2018, **8**, 4266–4277.
44 A. Thakur, P. Devi, S. Saini, R. Jain, R. K. Sinha and P. Kumar, *ACS Sustainable Chem. Eng.*, 2018, **7**(1), 502–512.
45 P. Luo, C. Li and G. Shi, *Phys. Chem. Chem. Phys.*, 2012, **14**, 7360–7366.
46 T. B. Devi and M. Ahmaruzzaman, *Chem. Eng. J.*, 2017, **317**, 726–741.
47 Y. Wang, R. Liang, W. Liu, Q. Zhao, X. Zhu, L. Yang, P. Zou, X. Wang, F. Ding and H. Rao, *Sens. Actuators, B*, 2018, **273**, 1627–1634.
48 A. Kshirsagar, T. Khanna, V. Dhanwe, K. H. Kate and P. K. Khanna, *J. Nanosci. Nanotechnol.*, 2018, **18**, 386–393.
49 Y.-Q. Zhang, D.-K. Ma, Y.-G. Zhang, W. Chen and S.-M. Huang, *Nano Energy*, 2013, **2**, 545–552.
50 W. Zhang, X. Zhang, Z. Zhang, W. Wang, A. Xie, C. Xiao, H. Zhang and Y. Shen, *J. Electrochem. Soc.*, 2015, **162**, H638–H644.
51 H. Bozetine, Q. Wang, A. Barras, M. Li, T. Hadjersi, S. Szunerits and R. Boukherroub, *J. Colloid Interface Sci.*, 2016, **465**, 286–294.
52 S. Muthulingam, K. B. Bae, R. Khan, I.-H. Lee and P. Uthirakumar, *J. Environ. Chem. Eng.*, 2016, **4**, 1148–1155.
53 N. Jallouli, L. M. Pastrana-Martínez, A. R. Ribeiro, N. F. Moreira, J. L. Faria, O. Hentati, A. M. Silva and M. Ksibi, *Chem. Eng. J.*, 2018, **334**, 976–984.
54 G. Lee, K. H. Chu, Y. A. Al-Hamadani, C. M. Park, M. Jang, J. Heo, N. Her, D.-H. Kim and Y. Yoon, *Chemosphere*, 2018, **212**, 723–733.
55 A. Smýkalová, B. Sokolová, K. Foniok, V. Matějka and P. Praus, *Nanomaterials*, 2019, **9**, 1194.
56 M.-C. Wu, A. Sápi, A. Avila, M. Szabó, J. Hiltunen, M. Huuhtanen, G. Tóth, Á. Kukovecz, Z. Kónya and R. Keiski, *Nano Res.*, 2011, **4**, 360–369.
57 S. Zhu, J. Zhang, X. Liu, B. Li, X. Wang, S. Tang, Q. Meng, Y. Li, C. Shi and R. Hu, *RSC Adv.*, 2012, **2**, 2717–2720.
58 E. B. Simsek, *Appl. Catal., B*, 2017, **200**, 309–322.
59 R. S. Varma, N. Thorat, R. Fernandes, D. Kothari, N. Patel and A. Miotello, *Catal. Sci. Technol.*, 2016, **6**, 8428–8440.
60 J. Patwari, A. Chatterjee, S. Sardar, P. Lemmens and S. K. Pal, *Phys. Chem. Chem. Phys.*, 2018, **20**, 10418–10429.

